Proton-nucleon spin-rotation and -depolarization parameters at 800 MeV

M. L. Barlett, G. W. Hoffmann, J. A. McGill,* B. Hoistad,† L. Ray, R. W. Fergerson, E. C. Milner, and J. A. Marshall‡
Department of Physics, The University of Texas at Austin, Austin, Texas 78712

J. F. Amann, B. E. Bonner, and J. B. McClelland
Los Alamos National Laboratory, Los Alamos, New Mexico 87545
(Received 19 March 1985)

Using a liquid deuterium target, 800 MeV quasielastic $\vec{p}+p$ and $\vec{p}+n$ spin-rotation and -depolarization parameters ($D_{SS}, D_{SL}, D_{LS}, D_{LL}, D_{NN}$) were determined over the center-of-momentum angular range 14.3°–69.2°. The $\vec{p}+p$ results are in good agreement with existing elastic results and predictions from phase shift analysis. The $\vec{p}+n$ results, in general, are not in agreement with predictions from phase shift solutions. Small corrections to previously reported $\vec{p}+p$ elastic observables are also discussed.

I. INTRODUCTION

A survey of the experimental $p+p$ elastic scattering observables at energies near 800 MeV reveals many recent, high quality measurements[1–16] which may be used in phase shift analyses to determine the $I=1$ phase shifts and scattering amplitudes at 800 MeV. A similar examination of the $p+n$ (or $n+p$) situation reveals a considerable absence of data. At forward angles only total cross section,[17,18] differential cross section,[19–21] and analyzing power[1,22] data have been obtained. These data, together with some back angle polarization and spin-transfer data,[23] comprise the entire pn data base near 800 MeV.

In order to help remedy the 800 MeV pn situation, we have determined forward angle ($14.3° \leq \theta_{c.m.} \leq 69.2°$) quasielastic ($LD_2$ target) $\vec{p}+n$ spin-rotation and -depolarization parameters, D_{ij}. Quasielastic $\vec{p}+p$ observables were also determined. Statistical errors in the D_{ij}'s are typically ± 0.03–0.05; relative point-to-point and absolute normalizations are $\leq \pm 2.5\%$ and $\leq \pm 2.0\%$, respectively. The quasielastic $\vec{p}+p$ results are in general agreement with those from previous elastic $\vec{p}+p$ measurements[2–4] and with predictions from current phase shift solutions.[24] This result suggests that the quasielastic data closely approximate free proton-nucleon data for the momentum transfer region spanned by the experiment ($0.8\ \text{fm}^{-1} \leq q \leq 3.5\ \text{fm}^{-1}$). However, the quasielastic $\vec{p}+n$ results are in general disagreement with current phase shift solutions,[24] particularly the spin-rotation parameters D_{SS} and D_{LL}, and indicate that the $I=0$ phases and pn scattering amplitudes are currently not well determined near 800 MeV.

II. EXPERIMENTAL

Data were obtained using the high resolution spectrometer (HRS) at the Los Alamos Clinton P. Anderson Meson Physics Facility (LAMPF) during LAMPF running cycles 29, 31, and 38. Beams of 800 ± 2 MeV polarized protons were incident on a 3.8 cm diam liquid deuterium (LD_2) target. The experimental setup was identical to that used for previously reported elastic $\vec{p}p$ measurements[4] except that a second arm, a recoil particle detection system, was used in conjunction with the HRS.

Forward scattered protons were analyzed by the HRS and then rescattered by the HRS focal plane polarimeter (FPP) carbon analyzer to determine polarizations at the focal plane. The recoil particle detection system, positioned at the conjugate free pN scattering angles, detected recoil protons and neutrons in coincidence with the HRS event, enabling separation of quasielastic $\vec{p}+p$ and $\vec{p}+n$ events. The focal plane polarizations were transformed to polarizations at the target after scattering (by taking spin precession caused by the HRS dipoles into account) and the D_{ij}'s were then calculated from these polarizations.

The recoil system consisted of an array of 7.5 cm × 7.5 cm × 15 cm plastic scintillators optically coupled to photomultipliers and mounted in a frame outside the 1 m radius scattering chamber (except for the 6° measurements as discussed below). The array viewed the target through a 0.25 mm thick stainless steel window. Most of the recoil particle phase space was subtended by the array at small HRS scattering angles. At larger angles the array spanned the peak of the recoil particle phase space. High voltage settings for the array photomultipliers were adjusted to yield reasonable neutron detection efficiencies (~ 10–25%, depending on recoil neutron energy). A set of thin plastic scintillators, viewed by photomultipliers on opposite ends, was positioned directly in front of the array (between the target and the array) and served to tag recoil protons.

The standard HRS-FPP trigger[4] was modified to require a recoil particle in coincidence with the event detected by the HRS. Specifically, an event registered in one of the thin recoil scintillators formed the recoil proton signal (PROTON), while an event which registered in a recoil array detector and did not register in the thin scintillators formed the recoil neutron signal (NEUTRON $=$ ARRAY$\cdot\overline{\text{PROTON}}$). These signals were then used in

a coincidence circuit with the HRS-FPP trigger to define quasielastic events for taping and off-line analysis. During cycles 29 and 31, quasielastic $\vec{p}\,p$ and $\vec{p}\,n$ data were obtained serially; in cycle 38, the quasielastic $\vec{p}\,p$ and $\vec{p}\,n$ data were obtained simultaneously by prescaling (1/10) the $\vec{p}\,p$ events. The prescaling ensured that roughly equal numbers of $\vec{p}\,p$ and $\vec{p}\,n$ events were written to tape.

In addition to the trigger modifications, a set of time-to-digital converters (TDC's) was used to record the relative timing between events detected in the HRS and the recoil detectors. The quasielastic event trigger (HRS·PROTON or HRS·NEUTRON) provided the start signal for each TDC channel. Event trigger timing was always determined by the second scintillator on the HRS focal plane. Stop signals were provided by the output pulses of leading edge discriminators connected to each array detector photomultiplier and from mean timed signals from the thin recoil charged particle detectors. Typical time difference spectra for recoil neutrons and protons are shown in Figs. 1 and 2.

During cycle 29 quasielastic $\vec{p}+p$ and $\vec{p}+n$ data were obtained at HRS laboratory angles of 10° and 15° using incident $\hat{n}$, $\hat{s}$, and $\hat{l}$ beam spin orientations (see Fig. 1 of Ref. 4 for a description of these orientations). For these measurements, the recoil system consisted of a 4×6 array and four thin (54 cm$\times$9 cm$\times$0.5 cm) horizontal counters located $\sim$1 m from the target.

In cycle 31, data were obtained at HRS laboratory angles of 6°, 20°, and 25° using $\hat{s}$ and $\hat{l}$ beam; data were obtained at laboratory angles of 6° and 30° using $\hat{n}$ beam. The recoil detection system was identical to the setup used in cycle 29, except for the 6° measurements. At 6° a single array detector and thin (10 cm$\times$10 cm$\times$1 cm) recoil charged particle detector were placed inside the scattering chamber approximately 20 cm from the target. In addition, the LD_2 target was offset 1 cm in the horizontal (scattering) plane in a direction perpendicular to the beam line and away from the recoil detection system. This reduced the target thickness in the recoil direction, and together with the alternate recoil detector setup, enabled the detection of low energy recoil protons at $\theta_{lab}=6°$ (approximately 12 MeV for a target nucleon initially at rest). The offset target configuration was used for all measurements during this period.

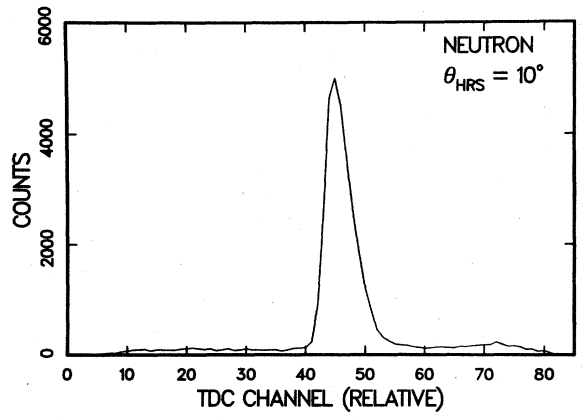

FIG. 1. Typical TDC histogram of time difference between HRS event and associated recoil neutron. The FWHM of the neutron peak is approximately 4 ns.

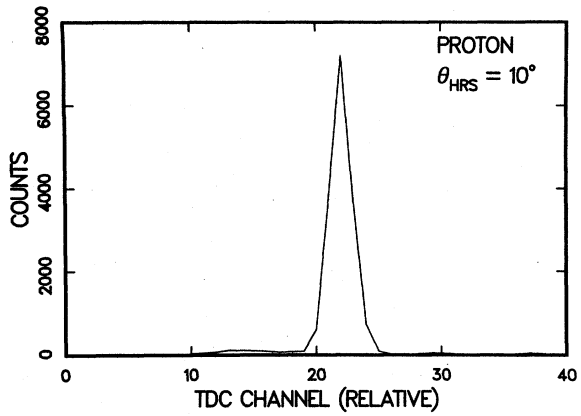

FIG. 2. Typical TDC histogram of the time difference between HRS event and associated recoil the proton. The FWHM of the proton peak is approximately 2 ns.

Data obtained during cycle 38 served primarily to check some of the previous results. Quasielastic $\vec{p}+p$ and $\vec{p}+n$ data were obtained at laboratory angles of 10° and 25° using an $\hat{s}$ beam. Quasielastic $\vec{p}+n$ data were obtained at HRS laboratory angles of 6° and 8° and quasielastic $\vec{p}+p$ data were obtained at 8° using beams which were a mixture of $\hat{s}$- and $\hat{l}$-type polarizations. The recoil detection system consisted of a 2×2 array with two thin (19 cm$\times$9 cm$\times$0.6 cm) recoil charged particle detectors located in a scattering chamber insert approximately 40 cm from the target.

Other details of the experimental setup (data acquisition system, beam line polarimeter, integrated beam current monitors, quench ratio monitors) are the same as those discussed in Ref. 4. Beam polarizations were typically 75—85 % except during cycle 38 when beam polarizations were typically 60—70 %. For the $\hat{n}$, $\hat{s}$, and $\hat{l}$ beams, polarization direction [normal (N) or reverse (R)] was changed at the ion source every minute. For the mixed spin beam orientations, polarization direction was changed 30 times per second. Logic levels from the ion source were read by the HRS on-line data acquisition system and used to tag each recorded event according to beam spin orientation. The FPP carbon analyzer thickness ranged from 15 to 27 cm depending upon the forward scattered proton's kinetic energy.

III. DATA ANALYSES AND RESULTS

A. Off-line reduction for cycles 29 and 31

The off-line analysis of the cycle 29 and 31 data was similar to that described for previously reported elastic $\vec{p}\,p$ spin-rotation and -depolarization parameter measurements[4] with the exception that identification of recoil particle-type was necessary. TDC data words associated

with the recoil proton detectors were combined into one data word and TDC data words associated with the detector array were combined into another. Histograms of these data words (gated by appropriate software tests) showed time-correlated coincidences between the HRS event and the recoil protons and neutrons. A neutron software test required that only one array detector triggered for a given HRS event and that no proton detector triggered. The time difference spectra for the recoil neutrons contained a narrow ($\simeq$3—4 ns FWHM) coincidence peak (see Fig. 1) with a broad, smooth background underlying the peak. Likewise, another software test defined a recoil proton as any event that triggered a proton detector for a given HRS event. The time difference spectra for recoil protons (see Fig. 2) had the same general features as the recoil neutron spectra with the exception that the proton spectrum at a given angle generally had a larger peak-to-background ratio.

Gates set on the recoil neutron and proton time-of-flight (TOF) histograms enabled FPP polarization determinations for $\vec{p}p$ and $\vec{p}n$ events. The technique used was essentially the same as that outlined in Ref. 4. Polarizations were obtained corresponding to two regions in both TOF histograms: (1) the time correlated peak plus the underlying background, and (2) the background. Peak-to-background ratios varied from $\sim$2.5:1 to 16:1 for the $\vec{p}n$ data and from $\sim$5:1 to 50:1 for the $\vec{p}p$ data. Background corrected FPP polarizations were obtained as discussed in Ref. 4. Other details such as particle identification (PID), missing mass cuts, restrictions on the polar scattering angle in the FPP carbon analyzer, trajectory matching requirements, and FPP acceptance tests are discussed in Ref. 4.

Beam polarization, P_B, was measured using both the quench method and a beam line polarimeter. The ratio of the two measures of P_B was constant to a few percent, but not equal to 1.0. The quench method yielded larger values by 7.5% and 3.8% in cycles 29 and 31, respectively. The differences were presumably due to small tuning errors at the polarized ion source which are known to lead to anomalous quench ratio polarization values. The beam line polarimeter polarizations were used in the computation of the D_{ij}'s for $\hat{n}$- and $\hat{s}$-type incident beams. For the measurements using $\hat{l}$-type incident beam, quench monitor polarizations were used, corrected by the factors quoted above. Spin-rotation and -depolarization parameters obtained from cycle 29 and 31 measurements were computed using FPP cone test acceptance cuts[25,26] and averaged over the full acceptance of the HRS as in the previous elastic $\vec{p}p$ analysis.[4] Results of the measurements for quasielastic scattering are shown as crosses in Figs. 3—12. Phase shift predictions shown in the figures are discussed in Sec. III E. The data are listed in Table I.

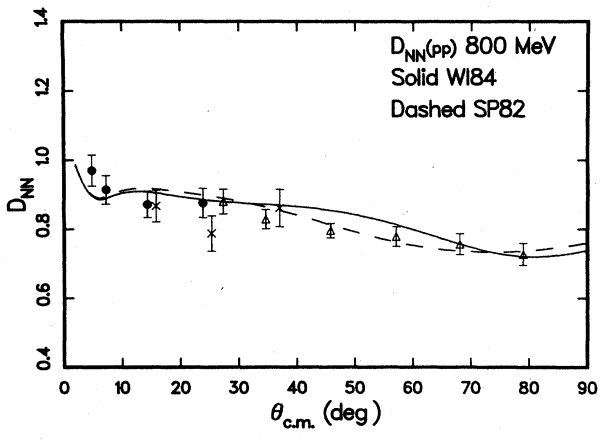

FIG. 3. The 800 MeV elastic $\vec{p}p$ D_{NN} results (solid dots) and quasielastic $\vec{p}p$ results (crosses) from this experiment are compared with those of Ref. 2 (open triangles) and phase shift predictions from Ref. 24. For visual clarity, the crosses are offset + 1.5°.

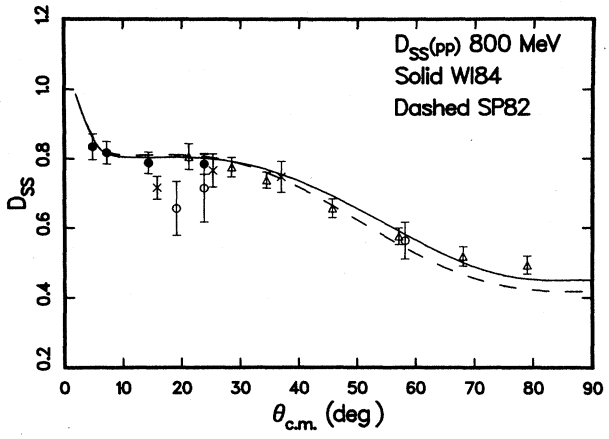

FIG. 4. The 800 MeV elastic $\vec{p}p$ D_{SS} results (solid dots) and quasielastic $\vec{p}p$ results (crosses and open circles) from this experiment are compared with those of Ref. 2 (open triangles) and phase shift predictions from Ref. 24. For visual clarity, the crosses are offset + 1.5°.

B. Off-line reduction for cycle 38

Off-line analysis of the $\hat{s}$-type incident beam runs was identical to that described above. However, for the measurements of the spin-rotation parameters at laboratory angles of 6° and 8°, the analysis differed somewhat from this procedure because the beam contained a mixture of $\hat{s}$- and $\hat{l}$-type components. For this "mixed spin" beam, the polarization components after scattering (at the target) are related to the two spin rotations which occur in the scattering process:

$$P_{s'}=D_{SS}P_B(\hat{s})+D_{LS}P_B(\hat{l}) \tag{1a}$$

and

$$P_{l'}=D_{LL}P_B(\hat{l})+D_{SL}P_B(\hat{s})\ . \tag{1b}$$

Here $P_{s'}$ ($P_{l'}$) is the polarization in the $\hat{s}'$ ($\hat{l}'$) direction after scattering and $P_B(\hat{s})$ [$P_B(\hat{l})$] is the incident beam polarization component in the $\hat{s}$ ($\hat{l}$) direction (see Fig. 1 of Ref. 4 for a definition of these coordinate systems). In or-

TABLE I. Quasielastic (LD_2 target) spin-rotation and -depolarization parameters for $\vec{p}p$ and $\vec{p}n$ at 800 MeV.

θ_{lab} (deg)	$\theta_{c.m.}$ (deg)	D_{NN} ($\vec{p}p$)	ΔD_{NN}($\vec{p}p$)	D_{NN}($\vec{p}n$)	ΔD_{NN}($\vec{p}n$)
6.0	14.3	0.867	±0.046	0.923	±0.055
10.0	23.8	0.788	0.051	0.879	0.061
15.0	35.5	0.861	0.054	0.894	0.076
30.0	69.2			0.760	0.244
θ_{lab} (deg)	$\theta_{c.m.}$ (deg)	D_{SS} ($\vec{p}p$)	ΔD_{SS}($\vec{p}p$)	D_{SS}($\vec{p}n$)	ΔD_{SS}($\vec{p}n$)
6.0	14.3	0.716	±0.033	0.523	±0.037
6.0	14.3			0.510	0.055
8.0	19.1	0.656	0.078	0.583	0.046
10.0	23.8	0.766	0.048	0.646	0.046
10.0	23.8	0.715	0.098	0.589	0.055
15.0	35.5	0.748	0.045	0.749	0.050
20.0	47.0			0.799	0.054
25.0	58.2			0.879	0.076
25.0	58.2	0.563	0.053	0.742	0.085
θ_{lab} (deg)	$\theta_{c.m.}$ (deg)	D_{SL} ($\vec{p}p$)	ΔD_{SL}($\vec{p}p$)	D_{SL}($\vec{p}n$)	ΔD_{SL}($\vec{p}n$)
6.0	14.3	0.094	±0.021	−0.287	±0.037
6.0	14.3			−0.105	0.061
8.0	19.1	0.167	0.087	−0.248	0.048
10.0	23.8	−0.050	0.029	−0.347	0.043
10.0	23.8	−0.223	0.109	−0.329	0.059
15.0	35.5	−0.158	0.023	−0.399	0.040
20.0	47.0			−0.405	0.045
25.0	58.2			−0.397	0.064
25.0	58.2	−0.249	0.046	−0.360	0.076
θ_{lab} (deg)	$\theta_{c.m.}$ (deg)	D_{LS} ($\vec{p}p$)	ΔD_{LS}($\vec{p}p$)	D_{LS}($\vec{p}n$)	ΔD_{LS}($\vec{p}n$)
6.0	14.3	−0.035	±0.021	0.199	±0.031
6.0	14.3			0.242	0.049
8.0	19.1	−0.116	0.064	0.284	0.038
10.0	23.8	0.020	0.023	0.385	0.040
15.0	35.5	0.140	0.018	0.409	0.037
20.0	47.0			0.458	0.046
25.0	58.2			0.452	0.058
θ_{lab} (deg)	$\theta_{c.m.}$ (deg)	D_{LL} ($\vec{p}p$)	ΔD_{LL}($\vec{p}p$)	D_{LL}($\vec{p}n$)	ΔD_{LL}($\vec{p}n$)
6.0	14.3	0.815	±0.052	0.535	±0.048
6.0	14.3			0.505	0.073
8.0	19.1	0.844	0.102	0.612	0.056
10.0	23.8	0.699	0.049	0.633	0.054
15.0	35.5	0.663	0.039	0.705	0.050
20.0	47.0			0.654	0.052
25.0	58.2			0.601	0.064

der to determine the spin-rotation parameters, it is necessary to make measurements with two different incident polarization directions containing mixtures of the "pure" spin components, $\hat{s}$ and $\hat{l}$.

For the $\theta_{lab}=6°$ and 8° measurements, two orthogonal incident polarization directions ($\hat{u}$,$\hat{v}$) lying in the plane defined by the $\hat{s}$ and $\hat{l}$ unit vectors were used. The unit polarization vectors are shown in Fig. 13. The rotation angle, θ_R, of the $\hat{v}$-type beam relative to the incident beam direction was determined to be 39°±0.1° from comparisons of beam spin orientations in other LAMPF beam lines[27] and beam transport properties of the HRS channel.

Data reduction for the "mixed spin" measurements was analogous to that discussed above with the exception that the spin-rotation parameters were functions of the incident and final polarizations of *both* the $\hat{u}$- and $\hat{v}$-type measurements. If one takes into account outgoing spin precession due to the HRS dipole fields and out-of-plane scattering effects as discussed in Ref. 26, the spin-rotation parameters may be expressed to lowest order in ξ as

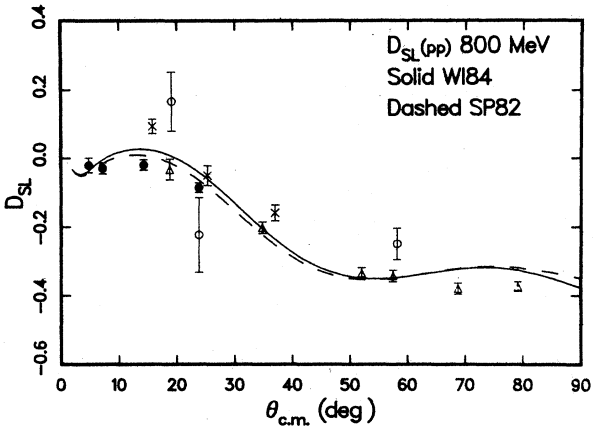

FIG. 5. The 800 MeV elastic $\vec{p}p$ D_{SL} results (solid dots) and quasielastic $\vec{p}p$ results (crosses and open circles) from this experiment are compared with those of Ref. 3 (open triangles) and phase shift predictions from Ref. 24. For visual clarity, the crosses are offset + 1.5°.

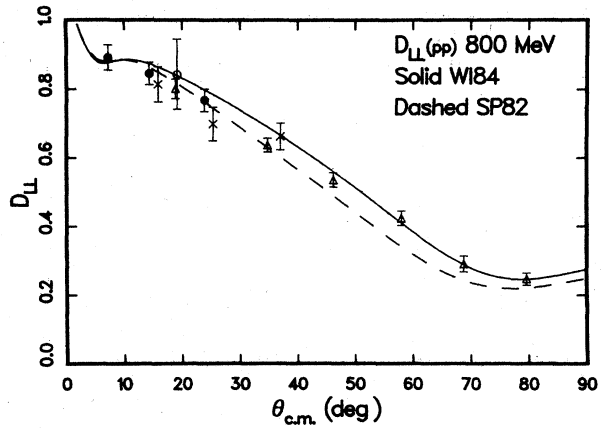

FIG. 7. The 800 MeV elastic $\vec{p}p$ D_{LL} results (solid dots) and quasielastic $\vec{p}p$ results (crosses and open circles) from this experiment are compared with those of Ref. 3 (open triangles) and phase shift predictions from Ref. 24. For visual clarity, the crosses are offset + 1.5°.

$$D_{SS}=D_{ss'}=R=\frac{\sin\theta_R}{2P_B(\hat{\mathbf{v}})\cos^2\xi_v}(P^{(+)}_{s'(v),\mathrm{FP}}-P^{(-)}_{s'(v),\mathrm{FP}}) + \frac{\cos\theta_R}{2P_B(\hat{\mathbf{u}})\cos^2\xi_u}(P^{(+)}_{s'(u),\mathrm{FP}}-P^{(-)}_{s'(u),\mathrm{FP}}) , \tag{2}$$

$$D_{SL}=D_{s1'}=R' = \frac{\sin\theta_R}{2P_B(\hat{\mathbf{v}})\cos\xi_v\sin\chi_v}(P^{(+)}_{n'(v),\mathrm{FP}}-P^{(-)}_{n'(v),\mathrm{FP}}) + \frac{\cos\theta_R}{2P_B(\hat{\mathbf{u}})\cos\xi_u\sin\chi_u}(P^{(+)}_{n'(u),\mathrm{FP}}-P^{(-)}_{n'(u),\mathrm{FP}}), \tag{3}$$

$$D_{LS}=D_{1s'}=A=\frac{\cos\theta_R}{2P_B(\hat{\mathbf{v}})\cos\xi_v}(P^{(+)}_{s'(v),\mathrm{FP}}-P^{(-)}_{s'(v),\mathrm{FP}}) - \frac{\sin\theta_R}{2P_B(\hat{\mathbf{u}})\cos\xi_u}(P^{(+)}_{s'(u),\mathrm{FP}}-P^{(-)}_{s'(u),\mathrm{FP}}) , \tag{4}$$

and

$$D_{LL}=D_{11'}=A'=\frac{\cos\theta_R}{2P_B(\hat{\mathbf{v}})\sin\chi_v}(P^{(+)}_{n'(v),\mathrm{FP}}-P^{(-)}_{n'(v),\mathrm{FP}}) - \frac{\sin\theta_R}{2P_B(\hat{\mathbf{u}})\sin\chi_u}(P^{(+)}_{n'(u),\mathrm{FP}}-P^{(-)}_{n'(u),\mathrm{FP}}) . \tag{5}$$

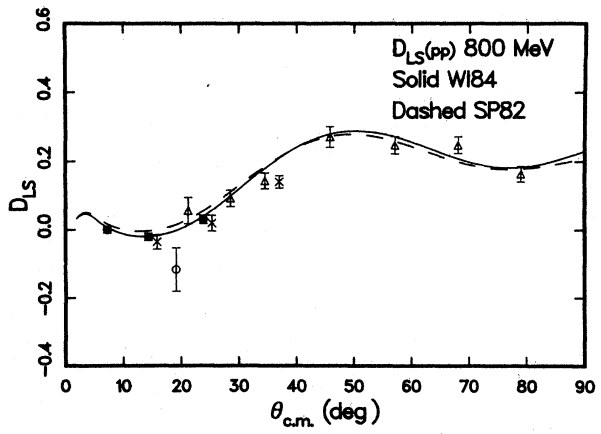

FIG. 6. The 800 MeV elastic $\vec{p}p$ D_{LS} results (solid dots) and quasielastic $\vec{p}p$ results (crosses and open circles) from this experiment are compared with those of Ref. 2 (open triangles) and phase shift predictions from Ref. 24. For visual clarity, the crosses are offset + 1.5°.

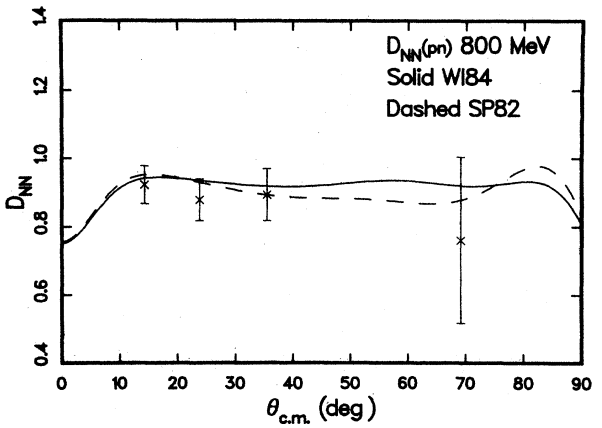

FIG. 8. The 800 MeV quasielastic $\vec{p}n$ D_{NN} results are compared with phase shift predictions from Ref. 24.

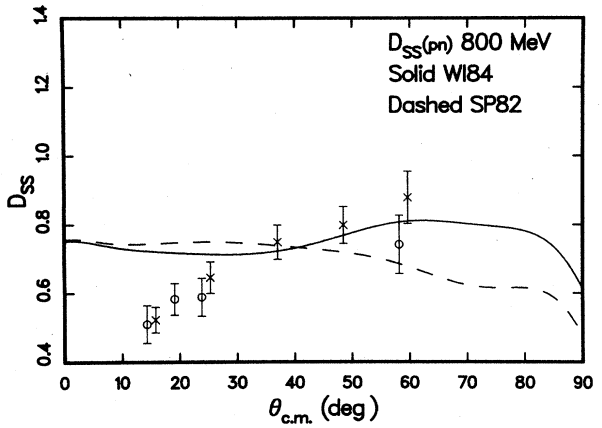

FIG. 9. The 800 MeV quasielastic $\vec{p}n$ D_{SS} results are compared with phase shift predictions from Ref. 24. The crosses are results from cycles 29 and 31; the open circles are from cycle 38. For visual clarity, the crosses are offset + 1.5°.

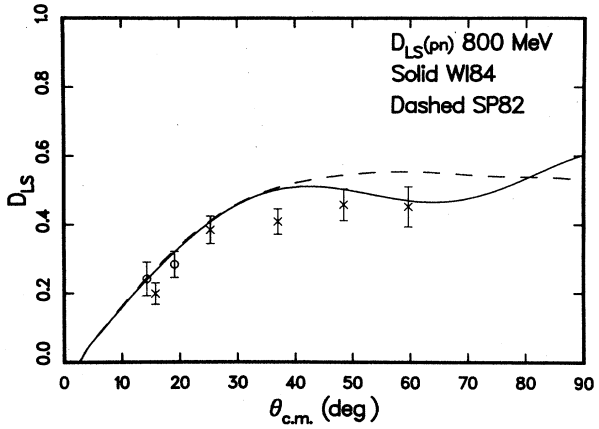

FIG. 11. The 800 MeV quasielastic $\vec{p}n$ D_{LS} results are compared with phase shift predictions from Ref. 24. The crosses are results from cycles 29 and 31; the open circles are from cycle 38. For visual clarity, the crosses are offset + 1.5°.

Here $P^{\pm}_{n'(v),\mathrm{FP}}$ ($P^{\pm}_{n'(u),\mathrm{FP}}$) and $P^{\pm}_{s'(v),\mathrm{FP}}$ ($P^{\pm}_{s'(u),\mathrm{FP}}$) are the background-corrected polarizations in the $\hat{n}'_{\mathrm{FP}}$ and $\hat{s}'_{\mathrm{FP}}$ directions (as defined in Fig. 1 of Ref. 4; FP denotes measurements at the focal plane) for $\hat{v}$- ($\hat{u}$-) type incident beam, the + (−) indicates normal (reverse) beam polarization, $P_B(\hat{v}$ or $\hat{u})$ is the incident beam polarization in the $\hat{v}$ or $\hat{u}$ direction, $\xi_{v,u}$ is the out-of-plane scattering angle at the target, and $\chi_{v,u}$ is the precession angle for $\hat{v}$- or $\hat{u}$-type incident beam. We have assumed that

$$P_B^{+}(\text{normal}) = -P_B^{-}(\text{reverse}) = P_B$$

and that the sines and cosines of ξ and χ are averaged over the events. Equations (2)—(5) show that instrumental asymmetries cancel to first order when D_{SS}, D_{SL}, D_{LS}, and D_{LL} are calculated in this manner.

For each run, beam polarization, $P_B(\hat{v}$ or $\hat{u})$, was calculated from the $\hat{s}$ component of the incident beam polarization determined by the beam line polarimeter and the quoted beam polarization rotation angle, θ_R. The spin-rotation parameters were computed using FPP cone test acceptance cuts. For a given run the scattering angle was taken as the central HRS angle (the HRS acceptance in the plane of scattering is about ±0.75°). Results from cycle 38 are shown as open circles in Figs. 4—7 and 9—12 and are listed in Table I. Good overall agreement is seen with the earlier results except for the small angle $\vec{p}p$ parameters. These differences are believed to be due to the target not being offset during the cycle 38 measurements, and the substantial geometry dependent absorption (increased target thickness in the recoil direction) of the low energy recoil protons that resulted.

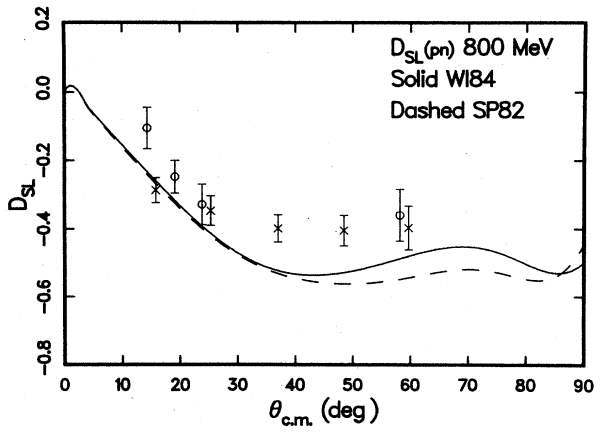

FIG. 10. The 800 MeV quasielastic $\vec{p}n$ D_{SL} results are compared with phase shift predictions from Ref. 24. The crosses are results from cycles 29 and 31; the open circles are from cycle 38. For visual clarity, the crosses are offset + 1.5°.

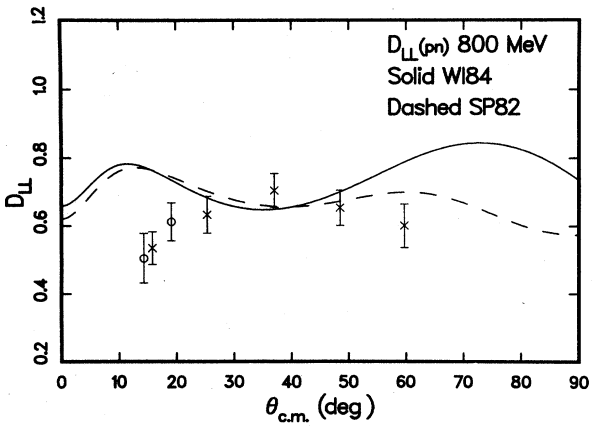

FIG. 12. The 800 MeV quasielastic $\vec{p}n$ D_{LL} results are compared with phase shift predictions from Ref. 24. The crosses are results from cycles 29 and 31; the open circles are from cycle 38. For visual clarity, the crosses are offset + 1.5°.

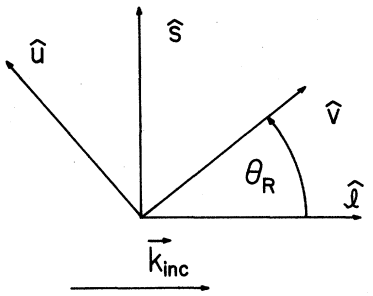

FIG. 13. The "mixed" incident beam spin directions $\hat{v}$ and $\hat{u}$ used in cycle 38 are shown relative to the "pure" spin directions $\hat{l}$ and $\hat{s}$. All vectors lie in the same plane. The directions shown are for NORMAL spin.

C. Corrections to small angle elastic $\vec{p}$p results

In the computation of the D_{ij}'s, corrections due to out-of-plane scattering were made to lowest order. The explicit lowest order dependence of these parameters on the out-of-plane scattering angle, ξ, is illustrated in Eqs. (3)—(7) of Ref. 4 for "pure spin" (incident $\hat{n}$, $\hat{s}$, or $\hat{l}$ beam polarizations) measurements and in Eqs. (2)—(5) of this work for "mixed spin" measurements. Terms not included in the computation are those which allow for mixing of the D_{ij}'s, specifically the mixing of D_{NN} and D_{SS}.[26] For the D_{ij}'s presented here these terms were shown to be negligible. However, for very forward angle measurements (typically $\theta_{lab} < 6°$) they may be significant. Such corrections were not made for previously reported elastic $\vec{p}$p D_{ij} results[4] which spanned HRS laboratory scattering angles from 2° to 10°.

The importance of the small angle correction traces to the azimuthal acceptance of the HRS (the range of ξ), which increases dramatically as the HRS scattering angle decreases. For the reported elastic $\vec{p}$p measurements, terms involving the azimuthal (out-of-plane) scattering angle, ξ, were event averaged by taking the average of the azimuthal angle and then evaluating the trigonometric functions (e.g., $\cos\overline{\xi}$, $\sin\overline{\xi}$, etc.) rather than evaluating the event-averaged trigonometric functions (e.g., $\overline{\cos\xi}$). The methods are basically equivalent when: (1) the average azimuthal angle is nearly 0°; (2) the event distribution of the azimuthal scattering angles is roughly flat and symmetric about 0°; and (3) the range of possible azimuthal angles is relatively small. These assumptions are generally valid, *except* at small HRS scattering angles.

In order to correct the small angle $\vec{p}$p results, the event-averaged trigonometric functions of the azimuthal scattering angle (e.g., $\overline{\cos\xi}$) were used rather than trigonometric functions of the event-averaged azimuthal scattering angle (e.g., $\cos\overline{\xi}$). Higher order terms which account for mixing of the parameters D_{NN} and D_{SS} as a function of the azimuthal angle were included and the spin-rotation and -depolarization parameters were recalculated. The results are listed in Table II and are shown as solid dots in Figs. 3—7. The effects of event averaging the trigonometric functions of ξ and including the higher order terms decreased rapidly as the scattering angle, θ_{lab}, increased. The largest effect, a change in D_{NN} of $+0.027$, occurred at $\theta_{lab}=2°$.

TABLE II. Revised (data were originally reported in Ref. 4) elastic spin-rotation and -depolarization parameters for $\vec{p}$p at 800 MeV.

θ_{lab} (deg)	$\theta_{c.m.}$ (deg)	D_{NN}	ΔD_{NN}
2.0	4.8	0.970	±0.045
3.0	7.2	0.914	0.041
6.0	14.3	0.872	0.038
10.0	23.8	0.876	0.042
θ_{lab} (deg)	$\theta_{c.m.}$ (deg)	D_{SS}	ΔD_{SS}
2.0	4.8	0.834	±0.037
3.0	7.2	0.817	0.032
6.0	14.3	0.788	0.031
10.0	23.8	0.785	0.030
θ_{lab} (deg)	$\theta_{c.m.}$ (deg)	D_{SL}	ΔD_{SL}
2.0	4.8	−0.020	±0.021
3.0	7.2	−0.029	0.016
6.0	14.3	−0.019	0.015
10.0	23.8	−0.085	0.014
θ_{lab} (deg)	$\theta_{c.m.}$ (deg)	D_{LS}	ΔD_{LS}
3.0	7.2	0.000	±0.009
6.0	14.3	−0.020	0.010
10.0	23.8	0.031	0.012
θ_{lab} (deg)	$\theta_{c.m.}$ (deg)	D_{LL}	ΔD_{LL}
3.0	7.2	0.893	±0.036
6.0	14.3	0.847	0.033
10.0	23.8	0.768	0.033

D. Systematic uncertainties

The errors associated with the D_{ij}'s of Tables I and II include statistical uncertainty, uncertainty in the background determination and subtraction, and the statistical uncertainty associated with determination of the incident beam polarization. Certain systematic effects must also be considered. The first of these is the uncertainty in the inclusive $\vec{p}$-^{12}C analyzing power of the FPP carbon analyzer and its effect on the D_{ij}'s. This uncertainty is discussed at length in Refs. 4 and 28 and leads to $\leq \pm 2.5\%$ uncertainties in the D_{ij}'s. This error is included in the quoted errors in Tables I and II as a point-to-point normalization uncertainty and is included in the error bars shown in Figs. 3—12.

Uncertainty in the absolute beam polarization is another source of systematic error. This uncertainty is estimated to be $\pm 1\%$ based on previous studies of the quench ratio technique[8,14] and beam line polarimeter-quench monitor consistency, except for the spin-rotation and -depolarization parameters obtained using $\hat{l}$-type beam (D_{LL} and D_{LS}). Here the uncertainty is estimated to be slightly larger ($\pm 2\%$) due to the renormalization of the quench ratios based on the $\hat{n}$- and $\hat{s}$-type runs. These errors are not included in the quoted errors and should be con-

sidered as an overall normalization uncertainty.

False asymmetries in the FPP may also lead to systematic errors. However, measurements of the outgoing polarizations for both normal and reverse incident beam spins facilitate computation of the spin-rotation and -depolarization parameters such that false asymmetries cancel to first order. Based on several sets of FPP calibration data taken at 0°, the measured false asymmetries were consistent with zero within their statistical determination (≤ 0.01).

Misidentification of the recoil particle-type can also contribute to systematic error. The importance of this effect depends primarily on: (1) the relative difference between the $\vec{p}p$ and $\vec{p}n$ quantities being measured, and (2) the absolute proton detection efficiency of the recoil proton detectors. The recoil proton detector efficiency is thought to be $\geq 99.9\%$ based on analyzing power measurements[1] performed during a portion of the experiment. Also, in the angular range spanned by this experiment, the spin-rotation and -depolarization parameters D_{SL}, D_{LS}, and D_{NN} for $\vec{p}p$ and $\vec{p}n$ are similar in magnitude, reducing the effects of recoil particle misidentification. The error introduced through particle misidentification is estimated to be negligible. A more detailed discussion of these effects is given in Ref. 1.

A self-consistency check of the data obtained in the experiment is possible since, in the nucleon-nucleon (NN) center-of-momentum system, $D_{s1}=-D_{1s}$.[29] Here the lowercase subscripts refer to the spin orientations in the NN center-of-momentum system and are related to the laboratory frame spin parameters through the relations

$$D_{s1}=D_{SS}\sin\theta_{\rm lab}+D_{SL}\cos\theta_{\rm lab} \tag{6a}$$

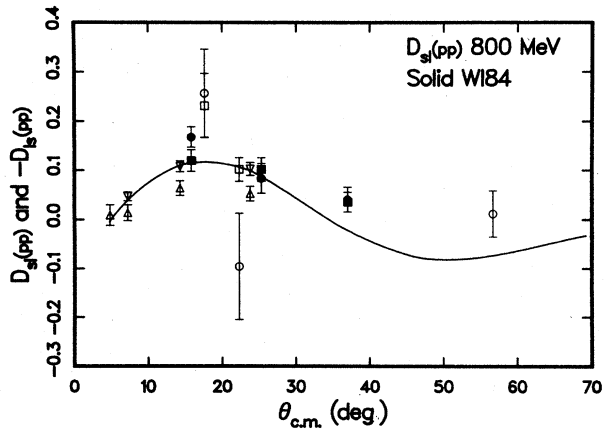

FIG. 14. The NN center-of-momentum spin-rotation parameters D_{s1} and $-D_{1s}$ obtained from the $\vec{p}p$ data at 800 MeV are compared with the WI84 phase shift prediction of D_{s1} from Ref. 24. The open triangles (inverted open triangles) are the symbols for the free $\vec{p}p$ parameter D_{s1} ($-D_{1s}$), the solid dots (solid squares) are the symbols for the quasielastic $\vec{p}p$ parameter D_{s1} ($-D_{1s}$) obtained from the cycle 29 and 31 data, and the open circles (open squares) are the symbols for the quasielastic $\vec{p}p$ parameter D_{s1} ($-D_{1s}$) obtained from the cycle 38 data. For visual clarity, the solid dots and squares are offset $+1.5°$; the open circles and squares are offset $-1.5°$.

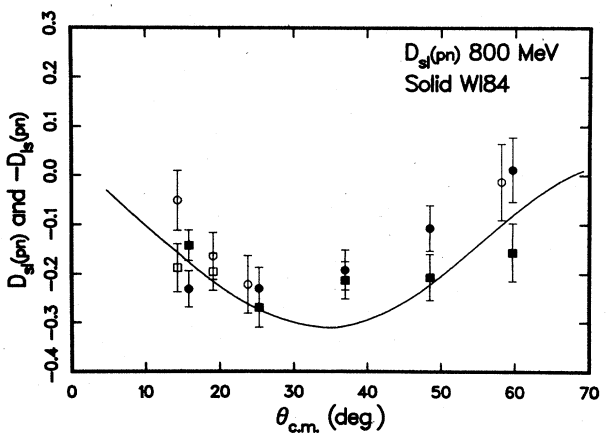

FIG. 15. The NN center-of-momentum spin-rotation parameters D_{s1} and $-D_{1s}$ obtained from the quasielastic $\vec{p}n$ data at 800 MeV are compared with the WI84 phase shift prediction of D_{s1} from Ref. 24. The solid dots (solid squares) are the symbols for the quasielastic $\vec{p}n$ parameter D_{s1} ($-D_{1s}$), obtained from the cycle 29 and 31 data, and the open circles (open squares) are the symbols for the quasielastic $\vec{p}n$ parameter D_{s1} ($-D_{1s}$) obtained from the cycle 38 data. For visual clarity, the solid dots and squares are offset $+1.5°$.

and

$$D_{1s}=D_{LS}\cos\theta_{\rm lab}-D_{LL}\sin\theta_{\rm lab}\,, \tag{6b}$$

where $\theta_{\rm lab}$ is the laboratory scattering angle. The results of such a check are shown in Fig. 14 (Fig. 15) for $\vec{p}p$ ($\vec{p}n$) where D_{s1}, $-D_{1s}$, and the WI84 phase shift predictions[24] for D_{s1} are compared. With the exception of the small angle quasielastic $\vec{p}p$ results ($\theta_{\rm lab}=8°,10°$) of cycle 38, the $\vec{p}p$ parameters appear to be consistent. The quasielastic $\vec{p}n$ parameters also appear to be generally self-consistent with differences between D_{s1} and $-D_{1s}$ typically less than or equal to about one standard deviation except at the largest angles.

E. Comparison with results of phase shift analysis

The main objective of the experiment was to provide data which would further constrain phase shift solutions at 800 MeV, particularly in the $I=0$ channel. The spin-rotation and -depolarization results of Tables I and II were included in a global phase shift analysis by Arndt.[24] Predictions from the resulting phase shift solution (WI84) are shown as the solid curves of Figs. 3–12. Also shown as dashed curves in these figures are predictions from an earlier solution[24] (SP82). Good agreement is seen between previously reported free $\vec{p}p$ parameters,[2,3] the free and quasielastic $\vec{p}p$ parameters from this experiment, and the phase shift predictions. Additional $\vec{p}p$ experiments will likely lead to only slight changes in the $I=1$ phases.

Poorer agreement is seen between the $\vec{p}n$ observables and the phase shift predictions. Only D_{NN} and D_{LS} are adequately described. The differences between the predictions from the solutions obtained before and after inclusion of the observables presented here are small in the

region of momentum transfer spanned by this experiment. It is therefore likely that other data in the data base and/or constraints built into this particular phase shift analysis dominate the determination of the solution at the lower momentum transfers. The observed disagreement between predictions from the current WI84 solution and the $\vec{p}n$ results from this experiment indicates that the pn scattering amplitudes at 800 MeV are not well determined. Measurements of additional observables at and near this energy are needed to resolve the discrepancies.

F. Comments on final state interactions and Fermi motion averaging

At intermediate energies where target nucleon binding effects are small (for deuterium), one expects the primary differences between elastic and quasielastic scattering to arise from: (1) the final state interaction (FSI) involving the spectator nucleon and (2) Fermi motion averaging. Qualitative arguments[30] have been given as to why little difference is expected at $E_p = 800$ MeV for momentum transfer ≥ 0.8 fm^{-1}. Such effects are known to lead to negligible difference between free and quasifree (LD_2 target) $\vec{p}p$ and $\vec{p}n$ (or $n\vec{p}$) analyzing power data obtained at 800 MeV (Ref. 1) for the region of momentum transfer covered in this experiment. The same basic arguments apply when comparing elastic and quasielastic spin-rotation and -depolarization parameters. The good agreement (except for the small angle cycle 38 $\vec{p}p$ measurements as discussed) between elastic and quasielastic $\vec{p}p$ D_{ij} results also suggests that the quasielastic $\vec{p}n$ D_{ij}'s will be negligibly different from those for free $\vec{p}n$. Of course the final state interaction can be different for p + p and p + n. In addition, phase shift predictions[24] of the spin-rotation and -depolarization parameters for a range of energies around 800 MeV corresponding to the limits of possible energies sampled by quasielastic scattering from deuterium (with a Fermi momentum of 45 MeV/c [732—872 MeV, with a mean energy of 806 MeV (Ref. 1)]) vary smoothly and almost linearly with energy at a fixed momentum transfer. Averaging over such an energy dependent distribution leads to the free scattering values.[1]

IV. SUMMARY AND CONCLUSIONS

We have presented new small-to-medium momentum transfer spin-rotation and -depolarization parameters for quasielastic (LD_2 target) $\vec{p}p$ and $\vec{p}n$ scattering at 800 MeV and refined elastic $\vec{p}p$ results from a previously reported experiment.[4] The elastic and quasielastic $\vec{p}p$ results are in good agreement with each other, with other existing results,[2,3] and with current phase shift solutions.[24] The agreement suggests that overall systematic uncertainties are small, that final state interaction and Fermi motion effects are small, and that the current pp ($I=1$) solution appears to be well determined near 800 MeV. The $I=0$ part of the current pn solution appears to be less accurately determined as evidenced by its failure to even qualitatively describe some of the pn D_{ij}'s. The phase shift analysis appears to be relatively insensitive to the new experimental input. Additional high quality $\vec{p}n$ data at and near 800 MeV are most likely required if the systematic discrepancies between experiment and phase shift solutions are to be resolved.

This work was supported in part by the U.S. Department of Energy and The Robert A. Welch Foundation.

*Present address: Los Alamos National Laboratory, Los Alamos, NM 87545.
†Present address: Gustaf Werner Institute, Uppsala, Sweden.
‡Present address: Southwest Research Institute, San Antonio, TX 78284.

[1] M. L. Barlett *et al.*, Phys. Rev. C **27**, 682 (1983).
[2] M. W. McNaughton *et al.*, Phys. Rev. C **25**, 1967 (1982).
[3] C. L. Hollas *et al.*, Phys. Rev. C **30**, 1251 (1984).
[4] M. L. Barlett *et al.*, Phys. Rev. C **30**, 279 (1984).
[5] F. Irom, G. J. Igo, J. B. McClelland, and C. A. Whitten, Jr., Phys. Rev. C **25**, 373 (1982).
[6] H. B. Willard *et al.*, Phys. Rev. C **14**, 1545 (1976).
[7] P. R. Bevington *et al.*, Phys. Rev. Lett. **41**, 384 (1978).
[8] M. W. McNaughton *et al.*, Phys. Rev. C **23**, 1128 (1981).
[9] A. Wriekat *et al.*, Phys. Lett. **97B**, 33 (1980); G. Pauletta *et al.*, Phys. Rev. C **27**, 282 (1983).
[10] M. W. McNaughton *et al.*, Phys. Rev. C **23**, 838 (1981).
[11] D. A. Bell *et al.*, Phys. Lett. **94B**, 310 (1980).
[12] I. P. Auer *et al.*, Phys. Rev. Lett. **41**, 1436 (1978).
[13] V. A. Andreev *et al.*, Gatchina Laboratory Report No. 656, 1981 (unpublished).
[14] M. W. McNaughton and E. P. Chamberlin, Phys. Rev. C **24**, 1778 (1981).
[15] T. S. Bhatia *et al.*, Phys. Rev. Lett. **49**, 1135 (1982).
[16] W. R. Ditzler *et al.*, Phys. Rev. D **27**, 680 (1983); **29**, 2137 (1984).
[17] T. J. Devlin *et al.*, Phys. Rev. D **8**, 136 (1973).
[18] P. W. Lisowski *et al.*, Phys. Rev. Lett. **49**, 255 (1982).
[19] R. Carlini *et al.*, Phys. Rev. Lett. **41**, 1341 (1978).
[20] M. L. Evans *et al.*, Phys. Rev. Lett. **36**, 497 (1976).
[21] M. Jain *et al.*, Phys. Rev. C **30**, 566 (1984).
[22] C. Newsom, Ph.D. thesis, The University of Texas at Austin, 1980 (unpublished).
[23] R. D. Ransome *et al.*, Phys. Rev. Lett. **48**, 781 (1982).
[24] R. A. Arndt *et al.*, Phys. Rev. D **28**, 97 (1983); private communication.
[25] D. Besset *et al.*, Nucl. Instrum. Methods **166**, 515 (1979).
[26] J. B. McClelland, J. F. Amann, W. D. Cornelius, H. A. Thiessen, B. Aas, and R. W. Fergerson, Los Alamos National Laboratory Report LA-UR-84-1671, 1984.
[27] M. W. McNaughton, private communication.
[28] R. D. Ransome *et al.*, Nucl. Instrum. Methods **201**, 315 (1982).
[29] J. Bystricky, F. Lehar, and P. Winternitz, J. Phys. (Paris) **39**, 1 (1978).
[30] D. R. Harrington, in *High Energy Physics and Nuclear Structure, Proceedings of the Fifth International Conference, Uppsala, 1973,* edited by G. Tibell (North-Holland, Amsterdam, 1974), pp. 118—122.